IOP Publishing Superconductor Science and Technology AUTHOR POSTPRINT
Published in 2020 *Supercond. Sci. Technol.* **33** 025006, https://doi.org/10.1088/1361-6668/ab601c

Anisotropy of the thermal conductivity of bulk melt-cast Bi-2212 superconducting tubes

Daria Szewczyk[1], Piotr Stachowiak[1], Jan Mucha[1], Mark Rikel[2], Jean-François Fagnard[3] and Philippe Vanderbemden[3]

[1] Institute for Low Temperature and Structure Research, Polish Academy of Sciences, Wrocław, Poland
[2] Deutsche-Nanoshicht GmbH (BASF), Rheinbach, Germany
[3] SUPRATECS group, "Montefiore" research unit, Department of Electrical Engineering and Computer Science, University of Liège, Belgium

E-mail: d.szewczyk@intibs.pl

Received 26 August 2019
Revised 26 November 2019
Accepted 9 December 2019
Accepted Manuscript online 9 December 2019

Abstract

We investigate experimentally the anisotropy of the temperature dependence of the thermal conductivity of bulk $Bi_2Sr_2CaCu_2O_8$ (Bi-2212) cylinders fabricated by the melt-cast process. The thermal conductivity $\kappa(T)$ along the axial and azimuthal directions are found to be equal within experimental uncertainty, while κ along the radial direction is found to be ~ 40% larger than the other two. The results are in qualitative agreement with the weak partial texture of such tubes, corresponding also to an anisotropy of the resistivity $\rho(T)$ above the critical temperature T_c. This resistivity anisotropy in the normal state is responsible for an anisotropy of the electronic contribution of thermal conductivity ($\Delta\kappa_e$), which is much smaller than the anisotropy $\Delta\kappa$ of the total thermal conductivity. This indicates an anisotropic contribution of the phonons. The temperature dependence of the specific heat $C(T)$ is also measured and shows that $C(T)/T$ exhibits a well-defined maximum close to T_c. The combination of these experimental data can be used for assessing the thermal effects in bulk melt-cast Bi-2212, and underline the importance of taking the anisotropy of κ into account, e.g. for predicting the self-heating when the material is subjected to losses.

Keywords: Thermal conductivity, Specific heat, Thermal properties, Bulk high-temperature superconductors, Cuprates

1. Introduction

Large superconducting materials made of bulk melt-cast processed (MCP) $Bi_2Sr_2CaCu_2O_{8+\delta}$ (Bi-2212) are characterized by a combination of properties that are attractive for large scale power systems [1,2]: they can be manufactured as large size samples (> 20 cm) of a priori arbitrary shape, they can sustain very large current densities exceeding 10^4 A/cm², and low contact resistance with silver can easily be achieved [3]. These materials have been the key components of the development of the first high-temperature superconducting fault current limiters [4-6] and were rapidly manufactured as current leads for low-T_c magnets [7]. The ability to manufacture sizable hollow superconducting parts make these materials also ideal candidates for passive magnetic shields [8]. Large melt- cast Bi-2212 hollow cylinders were demonstrated to shield axial magnetic fields of 1 tesla at 10 K [9], which is within the range of what can be achieved currently with MgB_2 cups or tubes [10-12] and bulk melt-processed YBCO [13]. The main advantage is that shielding is effective at levels that exceed the saturation magnetization (~ 0.7 T) of classic ferromagnetic shields made of mu-metal [14]. Stimulating prospects have also been opened recently by making so-called "magnetic cloaks", a variant of magnetic

shield in which flux density lines outside the cloak are not perturbed [15], that are based partially on bulk melt-cast Bi-2212 [16]. Passive magnetic shields and cloaks operating at high applied magnetic fields are particularly suited for applications involving particle beams [17-19].

In these systems, bulk Bi-2212 superconductors of large size are used under possibly large currents that are either injected or induced magnetically. When the currents or fields vary over time, the associated losses may lead to a temperature increase, which has therefore an impact on the thermal stability of the device. The combination of a large superconductor thickness and rather low thermal conductivity of high-temperature superconductors makes them prone to self-heating. Depending on the application, contradictory requirements can arise, as illustrated schematically in figure 1. We consider a bulk superconducting hollow cylinder used either as a current lead (left) or as a magnetic shield (right). When the superconductor is used as a current lead, it acts as a zero electrical resistance connection allowing a large transport current while ensuring a high thermal resistance between the low-temperature magnet and any external device. A *low* thermal conductivity along the axis of the tube, therefore, is desired to minimize the *axial* heat flux [20]. When the superconductor acts as a magnetic shield, the time varying magnetic field generates shielding currents (e.g. circumferential if the field is axial). If the field is ramped or varied sinusoidally, the losses appearing in the superconducting tube walls will be drained out towards the cryogenic coolant through the largest surface, i.e. the inner and outer walls of the tube. In this case a *high* thermal conductivity along the radial direction is therefore desired to maximize the *radial* heat flux. A reliable design of large scale systems based on such large tubes, therefore, requires the knowledge of the thermal properties along both axial and radial directions and should ideally take the material anisotropy into account.

The purpose of the present work is to investigate the anisotropy of the thermal conductivity of bulk Bi-2212 tubes fabricated by melt-cast process. This study is also motivated by recent quantitative texture analysis of these polycrystalline materials [21]. A <010> fiber texture with the axis parallel to the radial direction was deduced from XRD and neutron-diffraction studies. Though the texture was rather weak, not exceeding seven multiples of a random distribution, its combination with the extremely high intrinsic anisotropy of the Bi-2212 single grains [22] resulted in a noticeable anisotropy of the normal state resistivity, which was found to be a factor of two lower along the radial direction than along both axial and azimuthal directions of the tube [21]. These results agree with the qualitative picture in which the Bi-2212 platelets are preferentially oriented with their *c*-axes in a plane perpendicular to the radial direction [9]. It is therefore of interest to investigate to which extent the thermal conductivity of bulk melt-cast Bi-2212 is influenced by this anisotropy.

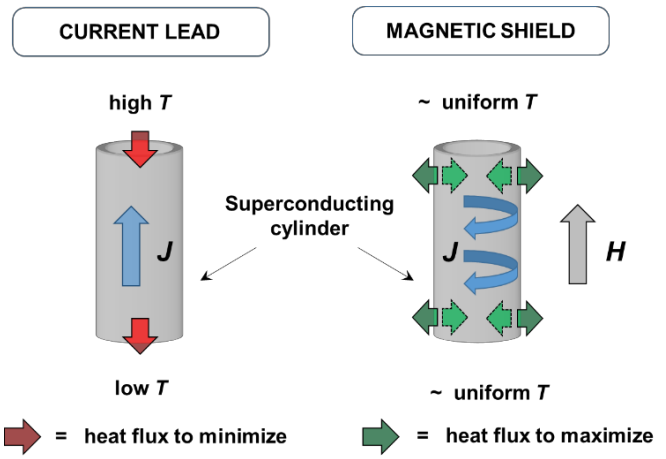

Fig. 1. Schematic illustration of bulk superconducting tube used either as a current lead or a magnetic shield. When the tube is used as a current lead, it is subjected to a transport current density *J* and a thermal gradient along its axis. A low thermal conductivity along the axis is desired to minimize the axial heat flux (in red). When the tube is used as a magnetic shield, the time varying applied field *H* generates shielding currents *J*. The associated power density is drained out through the lateral walls. A high thermal conductivity along the radial direction is desired to maximize the radial heat flux (in green).

2. Experiment

Experiments were carried out on a $Bi_2Sr_2CaCu_2O_{8+\delta}$ (Bi-2212) tube produced by melt-cast process at the Nexans Superconductors GmbH company and qualified for fault current limiter applications at 77 K. The details of the fabrication process are described in previous works [9, 21]. The tube was post-annealed to adjust the nominal oxygen content to $\delta \approx 0.235(2)$ close to the value (0.238) that was found to optimize the critical current density at 4.2 K [23]. This was achieved by slow (8°C/h) cooling after equilibration in air at 700°C for 5 h and annealing at 500°C for 96 h with subsequent furnace cooling (see [24,25] for the pO_2-temperaure map of oxygen contents in Bi-2212). The length of the tube was 150 mm, and the outer and inner diameters were 35 and 22.5 mm respectively (wall thickness = 6.25 mm).

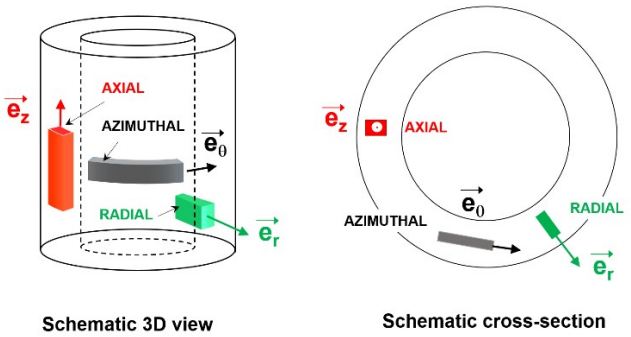

Fig. 2. Schematic illustration of the samples cut from the bulk Bi-2212 superconducting tube.

Three rectangular samples intended for electrical and thermal measurements were extracted from the Bi-2212 tube using a wire saw. Their long axis was oriented respectively along the axial, azimuthal and radial directions of the main tube, as shown schematically in figure 2. The samples were bar-shaped with respective dimensions 9.7 × 0.58 × 2.9 mm (axial); 15.5 × 1.5 × 1.2 mm (azimuthal) and 3.8 × 1.35 × 0.5 mm (radial). The melt-cast processed Bi-2212 material is known to contain a porous region, which for the tube of used thickness is mainly located in the zone between ~ 1 mm and ~ 2.7 mm from the inner wall of the tube. The axial and azimuthal samples were cut from an almost pore-free region situated in the inner zone of the tube wall that is characterized by the relatively uniform (less than 10% scatter) weak preferred orientation [23]. The radial sample

was cut to have smallest length acceptable in our system for the thermal conductivity measurements. The chosen region extending from ~ 1.2 mm to ~ 5 mm from the inner wall of the tube, may possibly include pores at the end close the inner wall. Such pores, however, were not visible from optical microscopy observations of the specimen surface. Electrical resistivity measurements were carried out in a Quantum Design Physical Property Measurement System (PPMS) with a DC Resistivity Option. The absolute accuracy of the resistance measurement is better than 0.5 %; the uncertainty

on the resistivity determination is estimated to ~ 5 % due to the uncertainty on the position of the voltage electrical contacts. Thermal conductivity measurements were carried out on specially designed heat-bath cryostat using a stationary

heat flux technique. The details of the setup can be found in references [26,27]. The standard deviation of the system is less than 2 %, but the overall uncertainty is around 5%, mostly due to the geometric errors on the sample dimensions and on the position of the thermocouples.

In addition, the temperature dependence of the specific heat was also measured on Quantum Design Physical Property Measurement System (PPMS) using the thermal relaxation method. As the heat capacity measurements are of a volume type only one kind of sample was investigated. The chosen one was reliably secured in the so-called “puck” (i.e. the measuring cell) with an Apiezon grease. The absolute accuracy of the heat capacity measurements was better than 1%; the uncertainty of the exact value determination is ~ 5 % stemming from the weight mass estimation of the sample.

3. Results and discussion

3.1. Electrical resistivity

We first examine the temperature dependence of the electrical resistivity ρ(*T*) along the azimuthal, axial and radial directions. Results are plotted in figure 3. All curves display a clear superconducting transition. The critical temperatures T_c for the three directions, defined here as the inflection points of the resistivity vs. temperature data, were determined by locating the maximum of dρ(T)/dT. This procedure leads to critical temperatures T_c of 85.8K, 84.3K, and 85K for the azimuthal, axial and radial directions respectively. It should be noted that these critical temperatures are ~ 7 K smaller than that of the initial tube, i.e. before post-processing [9] This confirms the strongly overdoped state. In the normal state, all curves display a quasi-linear metallic behaviour. The residual resistivity obtained by a linear extrapolation of the normal-state resistivity down to $T = 0$ is slightly negative for all directions.

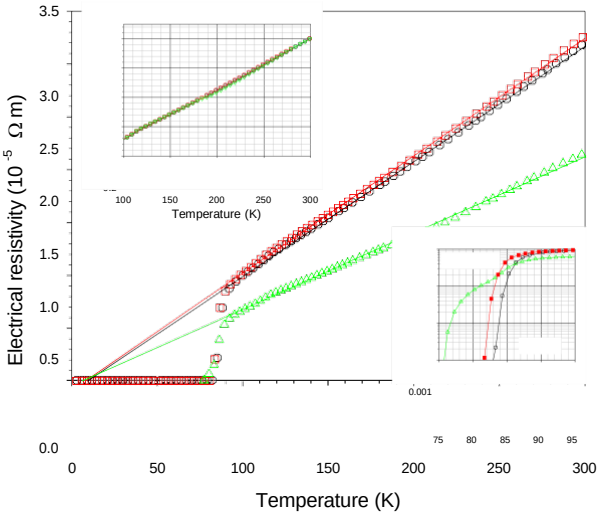

Fig. 3. Temperature dependence of electrical resistivity ρ measured on the melt-cast Bi-2212 rod for the axial (red), azimuthal (black) and radial directions (green) of the current. The data are obtained for a DC current of 5 mA injected in each sample. The arrow shows the location of the critical temperature T_c obtained from the derivative of the ρ(*T*) data. The upper-left inset shows the normal state resistivity normalized at $T = 300$ K. The lower-right inset visualizes the vicinity of the superconducting transition.

Such a behavior has been reported for the electrical resistivity along the *ab* planes of clean Bi-2212 single crystals [28]. The resistivity measured along the radial direction differs from the azimuthal and axial counterparts. The normal state resistivity along the radial direction is significantly lower (2.15 mΩ.cm at $T = 300$ K) than for the azimuthal and axial directions (3.20 mΩ.cm and 3.26 mΩ.cm at $T = 300$ K respectively). A slight ‘foot-like’ structure towards the bottom of the transition can be noticed along the radial direction, while the superconducting transitions along the azimuthal and axial directions do not exhibit any intermediate step. The foot may reflect non-uniformity of overdoping due to oxygen diffusion inside the outer layer of the tube upon furnace cooling from 500°C. Absence of such foot in specimens cut parallel to azimuthal and longitudinal directions could be a consequence of shunting these overdoped regions. The foot can be also a

signature of grain boundary effect [27]. Whatever the reason, the origin of this foot will not be discussed further. The resistivity values are comparable to those measured along the axis of bulk melt-cast Bi-2212 bars [29]. The anisotropy behavior depicted in figure 3 qualitatively agrees with results obtained on similar samples [21] in that the normal-state resistivity ratio ρ(axial,azimuthal) / ρ(radial) is very weakly temperature dependent with an average value equal to ~ 1.5, which is smaller than the ratio ~ 2.3 found by Dellicour *et al*. [21] for a similar tube of other dimensions (wall thickness ~7.5 mm) and, thus, different solidification microstructure. As found in [21], however, the normal state resistivity normalized at 300 K, $\rho(T)$ / ρ(300 K), is almost independent of the direction of the current (inset of figure 3). Additionally, these normalized data are very close to the normalized resistivity $\rho_{ab}(T)$ / ρ(300 K) measured along the *ab*-plane of similarly overdoped Bi-2212 single crystals [22, 30]. This suggests a negligible contribution of *c*-axis resistivity in the normal state, whatever the direction of the injected current.

3.2. Thermal conductivity

Figure 4 compares the thermal conductivity $\kappa(T)$ of the melt-cast Bi-2212 sample measured for the azimuthal, axial and radial directions. The axial and azimuthal set of data are remarkably similar, while the thermal conductivity along the radial direction is significantly higher than the other two. All curves display a well-defined maximum at T_{max} ~ 70 K, as well as positive and almost constant slope $d\kappa(T)/dT$ above T_c. The linear behavior of $\kappa(T)$ above T_c is usually observed for Bi-2212 compounds [31,32]. The arrow shows the location of the critical temperature obtained from the resistivity data. In the low temperature range (T < 20 K), all curves display a power law behavior $\kappa \sim T^n$, with n = 0.67 ±0.02 for all directions. Such a power law behavior $\kappa \sim T^n$ has been reported for other superconductors [33]. For T > 120 K, the difference Δκ between the thermal conductivity along the radial direction and the other two is almost temperature independent and equal to ~ 0.9 W m^{-1} K^{-1}. At T = 300 K, the thermal conductivity for the two sets of data are 3.2 W m^{-1} K^{-1} (radial) and 2.3 W m^{-1} K^{-1} (azimuthal and axial) respectively. One general feature to be noticed is the overall magnitude of the thermal conductivity. The data plotted in figure 3 are well within the range expected for Bi-2212 melt-cast processed samples [7] but are slightly higher than those reported recently for Bi-2212 textured rods fabricated by the Laser Floating Zone method [34]. The thermal conductivity is lower than that reported for $(RE)Ba_2Cu_3O_7$ where (RE) denotes a rare earth [24, 35-37]. This confirms the suitability of melt-cast processed Bi-2212 for current leads and their ability to maintain a thermal gradient between 4.2 K and 77 K [7]. Note also that the thermal conductivity is a factor of two smaller than the *ab*-plane thermal conductivity reported for Bi-2212 single crystals [25, 38-39].

Another parameter of interest allowing a comparison between samples is the ratio $\kappa(T_{max})/\kappa(T_c)$. From the results plotted in figure 4, this ratio is found to be 1.04, which is within the range found in polycrystalline and textured ceramics [40, 41]. It is however much lower than the value of ~ 1.16 reported for pure single crystals [28].

Next we turn to the anisotropy of the thermal conductivity, which presents similarities with the anisotropy of electrical conductivity. It is of interest, therefore, to estimate the temperature dependence of the electronic thermal conductivity $\kappa_e(T)$ above the critical temperature for the three directions of the heat flow. We assume the validity of the Wiedemann Franz law above 120 K, i.e. the temperature above which the contribution of fluctuations becomes negligible [28, 31]. One has $\kappa_e(T) = L_0\, T/\, \rho(T)$, where L_0 is the Lorenz number L_0 = 2.44 × 10^{-8} W Ω K^{-2} [42, 43]. The approximately linear temperature dependence of the resistivity above T_c yields a temperature-independent electronic thermal conductivity κ_e of 0.34 W m^{-1} K^{-1} and 0.23 W m^{-1} K^{-1} for the radial and axial / azimuthal directions respectively. At T = 300 K, the electronic contributions correspond respectively to 11 % and 10 % of the total thermal conductivity. Such values are similar to the 13% contribution reported for hot pressed Bi-2212 ceramics [44] and to a normal-state electronic contribution of 0.4 W m^{-1} K^{-1} reported for Bi-2212 polycrystalline samples [42]. The electronic contribution, however, is much lower than for Bi-2212 single crystals along the *ab* direction for which 30 % of the heat is carried out by electrons [28, 38]. The ratio (κ_{radial} / κ_{axial})

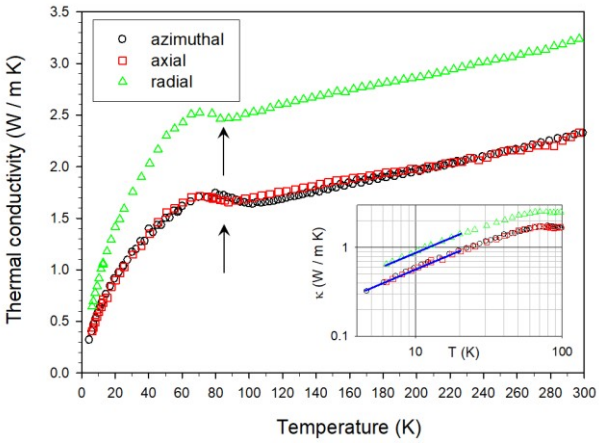

$\kappa(T)$

Fig. 4. Temperature dependence of thermal conductivity measured on the melt-cast Bi-2212 rod for the axial (red), azimuthal (black) and radial directions (green) of the heat flow. The arrow shows the location of the critical temperature T_c obtained from the $\rho(T)$ data. The inset show the same data plotted on a log-log scale. The lines are power law fits of the thermal conductivity κ as a function of temperature in the range 4 K < T < 20 K, i.e. $\kappa \sim T^n$, with n = 0.67±0.02.

calculated from our data at T = 300 K is 1.4. This value is much lower than the anisotropy ratio (κ_{ab} / κ_c) ~ 6 measured on Bi-2212 single crystals [45].

The difference $\Delta\kappa_e$ between the electronic contributions for the radial and axial / azimuthal directions above T_c is only 0.11 W m^{-1} K^{-1}, i.e. substantially lower than the measured difference $\Delta\kappa$ ~ 0.9 W m^{-1} K^{-1}. This result gives evidence that the anisotropy of the normal state electrical resistivity is not the only parameter to explain the anisotropy of the thermal conductivity plotted in figure 4. Since the main contribution to the total thermal conductivity arises from phonons, the anisotropy of the thermal conductivity reflects the different lattice contributions for the radial and axial / azimuthal directions. Another point to consider is the possible influence of the sample porosity on the thermal conductivity results. Due to the expected distribution of pores in the wall of the tube, the sample likely to be possibly affected by porosity is the radial one. The use of the Maxwell model [46] for the porosity correction consists in multiplying the measured thermal conductivity data by (1 +f / 2)/(1 - f), where f denotes the volume fraction of pores, assumed to be spherical and randomly distributed [47]. The consequence is that a porosity correction on the κ data for the radial sample would lead to an increase of the radial thermal conductivity, thereby increasing further the anisotropy of thermal conductivity. The practical conclusion to be drawn is that the anisotropic behavior observed in figure 4 is not an artefact caused by the possible porosity of the radial sample.

Interestingly, the measured anisotropy of the thermal conductivity is in line with the requirements for applications (cf. figure 1), i.e. a low thermal conductivity along the tube axis and a higher thermal conductivity along the radial direction, in order to drain out the losses through the lateral walls of the tube and minimize the temperature gradient in the walls. More precisely, the temperature distribution is expected to depend on the intrinsic thermal properties of the material and on the heat transfer between the superconductor and its thermal environment [48], the latter being dictated by the convective heat transfer U [49]. As an example, if the superconductor is placed in a low vacuum atmosphere (~ 10^{-2} mbar), the experimentally determined value of U is around 2 W m^{-2}K^{-1} [50]. For an infinite superconductor of radius a, the dimensionless Biot number (Ua / κ) is smaller than unity and the sample temperature can be assumed as uniform. In such a case, the particular value κ has little influence of the self-heating. On the opposite side, when the sample is in good thermal contact with the fluid, much higher values of U can be expected [51]. In this case, the heat equation, e.g. for hollow cylinders [52,53] predicts that the maximum sample temperature is inversely proportional to the thermal conductivity κ. Since the melt-cast processed Bi-2212 samples have a thermal conductivity anisotropy ratio of 1.4, ignoring this anisotropy can lead to a 40% error in the prediction of the internal temperature.

3.3. Specific heat

Finally, we investigate the temperature dependence of the specific heat. The $C(T)$ data are shown in the inset of figure 5, where the main plot shows the temperature dependence of C/T. One can observe a maximum in C/T around T ~ 90 K which resembles the C/T behavior, that was reported for Bi2212 single crystal [54]. At 300 K, i.e. the upper limit of the investigated temperature range, C = 333 J mol^{-1} K^{-1} which is still below the limit predicted by the Dulong-Petit law, i.e. 375 J mol^{-1} K^{-1}. In the range from 1.8 K to 6 K the experimental data follow the relation $C = C_1T+C_3T^3$. By fitting the experimental data in this temperature range, we can extract the Debye contribution – C_3T^3 to the specific heat. Using the classic formula from the Debye contribution [55]

$$C_{Debye} = \frac{12}{5}\pi^4 N_A k_B \left(\frac{T}{\theta_D}\right)^3,$$

where k_B is the Boltzmann constant, N_A the Avogadro number and θ_D the Debye temperature of the Bi-2212 sample, the latter can be calculated. It was found to be θ_D = 107.9 K. The obtained value is in fair agreement with the one computed for the Bi-2212 polycrystalline cuprates, which was $\theta_D \approx$ 93 – 105 K [56]. The $C(T)$ data plotted in figure 5 can be used for predicting the time dependence of the temperature rise in melt-cast Bi-2212 experiencing rapid temperature variations (dT/dt), a situation that would happen e.g. if the material is subjected to a rapidly varying current or applied magnetic field.

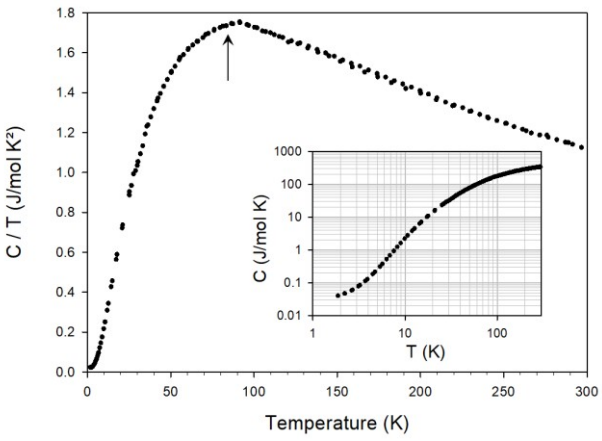

Fig. 5. Temperature dependence of the specific heat of the melt-cast Bi-2212 rod divided by the absolute temperature (C/T). The arrow shows the location of the critical temperature T_c obtained from the derivative of the $\rho(T)$ data. Inset: temperature dependence of the specific heat plotted on a log-log scale

4. Conclusion

The aim of the present work was to investigate the anisotropy of the thermal conductivity of bulk Bi-2212 tubes fabricated by melt-cast process. The thermal conductivity along the axial and azimuthal directions are found to be equal within experimental uncertainty, while the thermal conductivity along the radial direction is ~ 40% larger than the other two. The results are in qualitative agreement with the weak partial texture of melt-cast processed Bi-2212 tubes [21] that is also responsible for an anisotropy of the normal-state resistivity. In the present case the resistivity ratio between the axial / azimuthal directions with respect to the radial one was found to be very weakly temperature dependent with an average value equal to ~ 1.47. This resistivity anisotropy, yielding an anisotropy of the electronic contribution of the thermal conductivity, is not enough to account for the anisotropy of the total thermal conductivity. This fact points out the anisotropic contribution of the phonon thermal conductivity. Interestingly, the lower thermal conductivity along the radial direction is beneficial in draining out the possible losses through the lateral walls of the tube and in minimizing the temperature gradient in the walls. The set of data reported in the present paper is helpful in predicting accurately the temperature rise in large size melt-cast Bi-2212 sample exhibiting losses, as well as for the development of engineering applications involving these materials.

Acknowledgments

This work was supported in part by the collaboration programme between the FRS-FNRS (Belgium) and the PAN (Poland).

References

[1] Bock J., Elschner S. and Herrmann P. 1995 *IEEE Trans. Appl. Supercond.* **5** 1409
[2] Elschner S., Bock J., Obradors X., Puig T. and Granados X. 2019 *Superconducting Materials for SFCL* in: *Superconducting Fault Current Limiter: Innovation for the electric grids*, edited by P. Tixador, World Scientific Publishing, London, pp.61-76.
[3] Elschner S. and Bock J. 1992 *Adv. Mater.* **4** 242
[4] Bock J., Breuer F., Walter H., Noe M., Kreutz R., Kleimaier M., Weck K.-H. and Elschner S. 2004 *Supercond. Sci. Technol.* **17** S122
[5] Bock J., Bludau M., Dommerque R., Hobl A., Kraemer S., Rikel M. O. and Elschner S. 2011 *IEEE Trans. Appl. Supercond.* **21** 1202
[6] Dommerque R. et al. 2010 *Supercond. Sci. Technol*. **23** 034020
[7] Herrmann P.F. et al. 1993 *IEEE Trans. Appl. Supercond.* **3** 876
[8] Durrell J. H., Ainslie M. D., Zhou D., Vanderbemden P., Bradshaw T., Speller S., Filipenko M. and. Cardwell D. A. 2018 *Supercond. Sci. Technol.* **31** 103501
[9] Fagnard J. F., Elschner S., Bock J., Dirickx M., Vanderheyden B. and Vanderbemden P. 2010 *Supercond. Sci. Technol.* **23** 095012.
[10] Gozzelino L., Gerbaldo R., Ghigo G., Laviano F., Truccato M. and Agostino A., 2016 *Supercond. Sci. Technol.* **29** 034004
[11] Gozzelino L. et al. 2019 *Supercond. Sci. Technol*. **32** 034004
[12] Giunchi G., Barna D., Bajas H., Brunner K., Német A. and Petrone C. 2018 *IEEE Trans. Appl. Supercond.* **28** 6801705
[13] Wéra L., Fagnard J.-F., Namburi D. K., Shi Y., Vanderheyden B. and Vanderbemden P. 2017 *IEEE Trans. Appl. Supercond.* **27** 6800305
[14] Jiles D. 2015 *Introduction to Magnetism and Magnetic Materials*, 3rd Edition, CRC Press, Taylor and Francis
[15] Souc J., Solovyov M., Gömöry F., Prat-Camps J., Navau C. and Sanchez A. 2013 *New J. Phys.* **15** 053019
[16] Solovyov M., Šouc J., Gömöry F., Rikel M. O., Mikulášová E., Ušáková M. and Ušák E. 2017 *IEEE Trans. Appl. Supercond.* **27** 8800204
[17] Barna D. 2017 *Phys. Rev. Accel. Beams* **20** 041002
[18] Capobianco-Hogan K. G. et al. 2018 *Nucl. Instrum. Methods. Phys. Res. A* **877** 149
[19] Statera M., Balossinoa I., Barion L., Ciullo G., Contalbrigo M., Lenisa P., Lowry M. M., Sandorfi A. M. and Tagliente G. 2018 *Nucl. Instrum. Methods. Phys. Res. A* **882** 17
[20] Natividad E., Castro M., Burriel R. and Angurel L. A. 2006 *Journal of Thermal Analysis and Calorimetry* **84** 307
[21] Dellicour A., Vertruyen B., Rikel M. O., Lutterotti L., Pautrat A., Ouladdiaf B. and Chateigner D. 2017 *Materials* **10** 534
[22] Watanabe T., Fujii T. and Matsuda A. 1997 *Phys. Rev. Lett.* **79** 2113
[23] Dellicour A. 2014 "Physical properties/texture relationship in industrial melt-cast processed Bi-2212 bulk superconductors using quantitative texture analysis", PhD Thesis, University of Liege
[24] Majewski P. 2000, *J. Mater. Res.* **15** 854
[25] Schweizer T., Müller R., Bohac P. and Gauckler L. J. 1993 *Third EURO-CERAMICS. Vol. **2** Properties of ceramics* 611
[26] Jezowski A., Mucha J. and Pompe G. 1987 *J. Phys. D: Applied Physics* **20** 1500
[27] Marchal C., Fagnard J. F., Shi Y. H., Cardwell D. A., Mucha J., Misiorek H., Cloots R., Vertruyen B. and Vanderbemden P. 2013 *Supercond. Sci. Technol.* **26** 015006
[28] Ando Y., Takeya J., Abe Y., Nakamura K. and Kapitulnik A. 2000 *Phys. Rev. B* **62** 626
[29] Oikawa D., Higashi Y., Murotani H., Sugiura T., Andoh H. and T. Tsukamoto 2015 *IEEE Trans. Appl. Supercond.* **25** 6800304
[30] Yamada Y., Watanabe T. and Suzuki M. 2007 *Physica C* **460-462** 815
[31] Houssa M., Bougrine H., Stassen S., Cloots R. and Ausloos M., 1996 *Phys. Rev. B* **54** R6885
[32] Krishana K., Ong N. P., Li Q., Gu G. D. and Koshizuka N. 1997 *Science* **277** 83
[33] Mucha J., Pekała M., Szydłowska J., Gadomski W., Akimitsu J., Fagnard J.-F., Vanderbemden P., Cloots R. and Ausloos M. 2003 *Supercond. Sci. Technol*. **16** 1167
[34] Ozabaci M., Kizilaslan O., Madre M. A., Yakinci M. E. and Sotelo A. 2015 *J. Mater. Sci.: Mater. Electron.* **26** 3090
[35] Shams G. A., Cochrane J. W. and Russell J. G. 2000 *Physica C* **336** 205
[36] Fujishiro H. and Kohayashi S. 2002 *IEEE Trans. Appl. Supercond.* **12**
[37] Fujishiro H., Nariki S. and Murakami M. 2006 *Supercond. Sci. Technol*. **19** S447
[38] Crommie M. F. and Zettl A. 1990 *Phys. Rev. B* **41**, 10978

[39] Fujishiro H., Ikebe M., Naito T., Matsukawa M., Noto K., Shigaki I., Shibutani K., Hayashi S. and Ogawa R. 1994 *Physica C* **235–240** 1533
[40] Nakamae S. and Schwartz J. 1997 *IEEE Trans. Appl. Supercond*. **7** 1699
[41] Natividad E., Castro M., Burriel R., Angurel L. A., Diez J. C. and Navarro R 2002 *Supercond. Sci. Technol.* **15** 1022
[42] Houssa M., Ausloos M., Cloots R. and Bougrine H. 1997 *Phys. Rev. B* **56** 802
[43] Ikebe M., Fujishiro H., Naito T. and Noto K. 1994 *J. Phys. Soc. Japan* **63** 3107
[44] Peacor S. D. and Uher C. 1989 *Phys. Rev. B* **39** 11559
[45] Crommie M. F. and Zettl A. 1991 *Phys. Rev. B* **43** 408
[46] Maxwell J. C. A. 1954 *Treatise on Electricity and Magnetism*, Dover, NewYork
[47] Mucha J., Vertruyen B., Misiorek H., Ausloos M., Durczewski K. and Vanderbemden P. 2009 *J. Appl. Phys.* **105** 063501
[48] Tsukamoto O., Yamagishi K., Ogawa J., Murakami M. and Tomita M. 2005 *J. Mater. Process. Technol.* **161** 52.
[49] Sokolovsky V. and Meerovich M. 1998 *Physica C* **308** 215
[50] Vanderbemden P., Laurent P., Fagnard J.-F., Ausloos M., Hari Babu N. and Cardwell D. A. 2010 *Supercond. Sci. Technol.* **23** 075006.
[51] Mosqueira J., Cabeza O., Miguélez F., François M. X. and F. Vidal 1994 *Physica C* **235-240** 210
[52] Thorn R. J. and Simpson O. C. 1953 *J. Appl. Phys.* **24** 297
[53] Barletta A. and Zanchini E. 1995 *International Journal of Heat and Mass Transfer* **38** 2821
[54] Junod A., Wang Q., Tsukamoto T., Triscone G., Revaz B., Walker E. and Muller J. 1994 *Physica C* **229** 209
[55] Debye P. 1912 *Annalen der Physik* **344** 789
[56]Villiers P.de et al. 1992 *J. Phys.: Condens. Matter* **4** 9401